Kovove Mater. 61 2023 401–407
DOI: 10.31577/km.2023.6.401

Effect of heat treatment on the microstructure and fatigue behaviour of AISI 4130 steel

Jakub Poloprudský, Alice Chlupová*, Ivo Šulák, Karel Obrtlík

Institute of Physics of Materials, CAS, Žižkova 513/22, 616 00 Brno, Czech Republic

Received 9 June 2023, received in revised form 14 August 2023, accepted 18 August 2023

Abstract

AISI 4130 steel is widely used in the aircraft industry, mainly for frame structures. It is a medium carbon low-alloyed (25CrMo4) steel predetermined for precipitation of carbides in the microstructure during heat treatment. Six different heat treatments were applied to study the effect of the resulting microstructure (ferritic-pearlitic in a normalised state or martensitic with carbides in a hardened state) on the fatigue life of AISI 4130. Tension-tension cycling under force control was used to determine the *S-N* curve of flat specimens with a central circular notch. The best fatigue properties were achieved for the material state HT125, i.e., hardened & tempered to 125 ksi (863 MPa), exhibiting the maximum stress at a fatigue limit of 225 MPa, which is approximately 5–15 % better compared to the rest of the applied heat treatments. Microstructural investigations using scanning electron microscopy explained the acquired fatigue life results of AISI 4130 concerning different heat-treated conditions.

K e y w o r d s: medium carbon steel, heat treatment, fatigue life, microstructure, scanning electron microscopy

1. Introduction

AISI 4130 is a popular ultra-high-strength steel used since 1961 for rocket motor applications [1]. Nevertheless, it has a wide range of applications, from small bolts to the airframe structure of aircraft [2]. One of the key characteristics determining the application of the material is good resistance to cyclic stress [3], enabling the choice of the optimal steel microstructure for the given application or the use of the data for further numeric calculations. The microstructure and mechanical properties of a medium carbon low-alloyed (25CrMo4) steel strongly depend on the applied heat treatment. Carbon content predetermines the AISI 4130 steel for heat treatment, where the goal is to achieve the martensitic structure with a homogeneous distribution of fine carbides in the interior.

This work aimed to optimise the heat treatment to improve the fatigue endurance of AISI 4130 steel. The fatigue life in the form of *S-N* curves for notched specimens in various heat treatment states was analysed and related to microstructure observation. The hardened state HT125 exhibited the best fatigue properties, i.e., the highest conventional maximum stress at a fatigue limit of 225 MPa. Explanation of the fatigue life improvement is based on microstructural investigation using scanning electron microscopy.

*Corresponding author: e-mail address: chlupova@ipm.cz

2. Experiment

2.1. Material, heat treatment, and specimens

The specimens for fatigue life tests were fabricated from a 0.12″ ($T = 3.048$ mm) thick sheet of AISI 4130 steel (25CrMo4). AISI 4130 is a medium carbon, low alloy steel containing nominally 0.28–0.33 % C, 0.8–1.1 % Cr, and 0.15–0.25 % Mo as strengthening alloying elements. Flat specimens having a central circular notch with a diameter of $d = 4$ mm (according to the drawing shown in Fig. 1) with a length of 250 mm and flared ends with a width of 36 mm for clamping in flat hydraulic grips were used. The gauge length was 70 mm with a constant $W = 24$ mm width. The

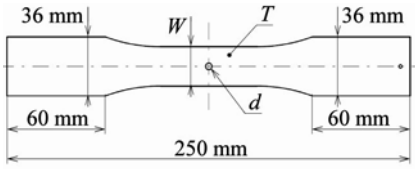

Fig. 1. Test specimen for fatigue life measurement.

dimensions of the test specimens in the gauge length (T, W, d) were used for stress calculations.

Test specimens were heat-treated to various conditions. Six different states of material were as follows: N = Normalized, HT90, HT125, and HT150 = Hardened & Tempered to 90, 125, and 150 ksi (i.e., 621, 863, and 1035 MPa), 2HT125 = Twice Hardened & Tempered to 125 ksi, and 2HT125N = Twice Hardened & Tempered to 125 ksi with Normalization. After heat treatment, the specimen surface was not mechanically treated.

2.2. Fatigue loading

Fatigue tests of notched specimens in various heat-treated conditions were performed at room temperature. The MTS 810 electro-hydraulic testing system with a capacity of ± 100 kN controlled by Teststar IIs digital electronics in force control mode was used for cyclic loading. A sinusoidal shape of the loading cycle was applied with a frequency of $f = 15$ Hz. During the test, maximum and minimum fatigue cycle force values $F_{\max}$ and $F_{\min}$ were kept constant with a parameter of asymmetry $R = 0.05$ ($R = F_{\min}/F_{\max}$). Cyclic loading was performed until the final fracture at the number of cycles N_f. The values of the load force $F_{\max}$ were chosen to obtain data on the fatigue life approximately in the interval of 5×10^3 to 5×10^6 cycles to fracture. The fatigue life for each type of heat treatment was measured on at least 12 test specimens. The aim was to investigate the fatigue life range of 5×10^3 through 5×10^6 cycles, assess the fatigue limit, locate the knee of the S-N curve, and describe both the upper and the lower branch of the curve.

2.3. Fatigue life methodology

The test methodology followed the standard for fatigue experiments with a constant amplitude of the controlled force acting on the axis of the specimen at room temperature [4]. The aim was to obtain the dependence of the maximum stress in the cycle $\sigma_{\max}$ on the number of cycles to fracture N_f for the chosen asymmetry of the cycle R, i.e., the S-N curve. In the area of a timed lifetime, the S-N dependence has the character of a straight line in bi-logarithmic representation, which can be approximated by the dependence:

$$\sigma_{\max} = A(N_f)^b, \tag{1}$$

where $\sigma_{\max}$ is the maximum stress, A is the fatigue strength coefficient, N_f is the number of cycles to fracture, and b is the fatigue strength exponent. The dependence can be modified according to the standard [5] into a shape:

$$\log N_f = (1/b) \log \sigma_{\max} - (1/b) \log A, \tag{2}$$

where fatigue life appears as a dependent variable. The parameters A and b, together with standard errors, were determined by regression analysis.

With a decrease in stress, some materials (typically steels) exhibit a change of dependence to an almost horizontal line at a service life of around 10^6 cycles. The corresponding stress value in this area is considered the fatigue limit. In this work, the fatigue limit is determined conventionally for a fatigue life of 5×10^6 cycles. The transition area between the linear dependence Eq. (2) in the bi-logarithmic representation and the horizontal line denoting the conventional fatigue limit was estimated based on fatigue life tests. Tests with a constant value of maximum stress in a cycle at a constant asymmetry parameter R leading to specimen fracture started at values of $\sigma_{\max}$ in the region between 500 and 600 MPa, depending on the strength (i.e., heat treatment) of the material. Tests continued with a decreasing value of $\sigma_{\max}$ up to the level where no failure (fatigue fracture) occurred even after the number of cycles of 5×10^6. In the following test, $\sigma_{\max}$ was reduced by 5–10 MPa, and if the fracture of the test specimen did not occur in 5×10^6 cycles ("run-out"), this reduced value was used to calculate the fatigue limit.

To determine the fatigue life curves of the notched specimens, at least 12 valid fatigue tests were performed for each material state. The applied stresses were calculated from the gross cross-section of the gauge length of the specimen $\sigma = F/(W \times T)$, i.e., outside the central circular notch. The stress $\sigma_{\max}$ was determined from the average value of the maximum force $F_{\max}$ from all cycles of the given test.

2.4. Microstructure observation

The thorough observation of microstructure after heat treatment was performed using a scanning electron microscope (SEM) Tescan LYRA 3 XMU FEG/SEMxFIB (TESCAN Brno, CZ) and electron backscattered diffraction (EBSD) method using a Symmetry S2 EBSD detector and Aztec crystal software (Oxford Instruments, UK). The metallographic samples were cut, mechanically ground and polished, and subsequently electropolished to highlight the presence of fine carbides. A mixture of acetic acid and perchloric acid was used as the electrolyte. The surface

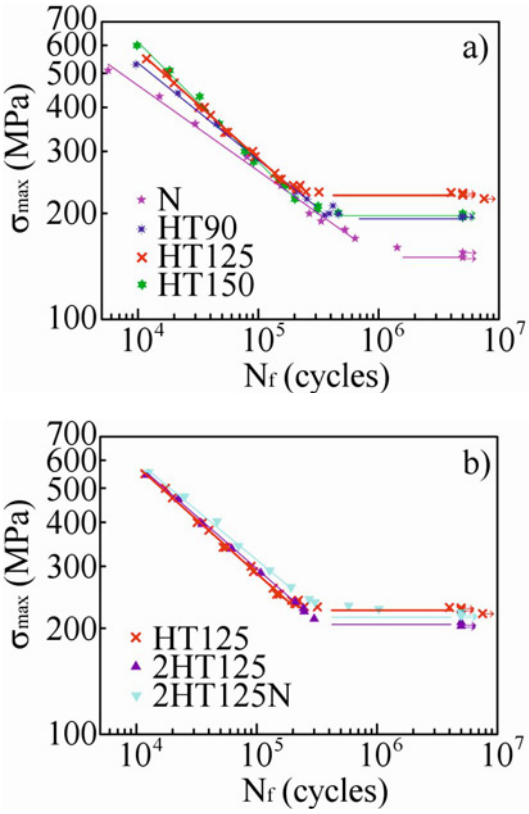

Fig. 2. Fatigue life curves of material AISI 4130 for six different states of heat treatment: (a) comparison of N, HT90, HT125, and HT150, (b) comparison of HT125 variants, i.e., HT125, 2HT125, and 2HT125N; arrows indicate run-outs.

for EBSD analysis was treated by chemical-mechanical polishing using colloidal silica suspension (OPS solution) with a particle size of 0.04 µm.

3. Results and discussion

Fatigue limit at symmetrical loading corresponds to stress amplitude σ_a for 5×10^6 cycles. In this work, where asymmetrical loading was applied, the fatigue life curves were expressed in the dependence of σ_{max} vs. N_f shown in Fig. 2. The fatigue limit at asymmetrical loading can be recalculated as follows:

$$\sigma_{m,f} = (1 - R)/2\sigma_{max,f}. \quad (3)$$

An arrow next to the symbol in the graphs means that the cycling of the specimen was interrupted at the number of cycles higher than 5×10^6 without fracture of the specimen (run-out). Since the experimental scatter of the measured data is relatively low, it was possible to distinguish the validity region of the linear dependence and the transition region well and establish the fatigue limit. Heat treatment HT125 represents the hot candidate for applying AISI 4130 steel for aircraft structural components. Therefore, increased attention was paid to this material state, and more fatigue tests were accomplished (see red data points). A comparison of HT125 with other heat treatments resulting in different strengths is shown in Fig. 2a. All hardened states in Fig. 2a (i.e., HT90, HT125, and HT150) exhibit better fatigue limits than the normalised state (N). Among hardened states, the heat treatment HT125 reaches the best fatigue limit. σ_{max} at asymmetrical cycle with $R = 0.05$ was approximately 225 MPa. Therefore, the fatigue limit determined according to Eq. (3) is $\sigma_{m,f} =$ 106.9 MPa and the stress range at the fatigue limit is 213.8 MPa.

All hardened states exhibit approximately 50 % higher fatigue limit than the N state. Also, other different variants of heat treatment based on HT125 were tested (see Fig. 2b). When various heat treatments based on hardening to 125 ksi are compared, i.e., HT125, HT2x125, and HT2x125N, the differences are minor (approximately 10 %); nevertheless, the best results concerning the fatigue limit are still reached for HT125. Although it is well documented that high levels of strength can be achieved with this material through appropriate heat treatment [6, 7], our investigation showed that increasing the strength to a level higher than 125 ksi does not lead to better fatigue resistance.

Table 1 summarises the stress domains of individual regions of fatigue life curves. The first interval of maximum stress, where the linear dependence from Eq. (2) is valid, creates the left part of *S-N* depen-

Table 1. The stress domains and parameters of fatigue life curves for various heat treatment states

Mat. state	$\sigma_{max,lin}$ (MPa)	$\sigma_{max,tr}$ (MPa)	$\sigma_{max,f}$ (MPa)	$\sigma_{m,f}$ (MPa)	$\sigma_{a,f}$ (MPa)	A (MPa)	b (–)
N	510–190	180–160	150	71.25	142.5	4610 ± 520	–0.249 ± 0.010
HT90	530–220	210–198	194	92.15	184.3	6780 ± 460	–0.275 ± 0.006
HT125	550–250	250–230	225	105.45	210.9	10290 ± 530	–0.312 ± 0.005
HT150	600–220	210–200	196	93.10	186.2	14500 ± 1700	–0.343 ± 0.010
2HT125	550–230	225–215	205	97.38	194.8	8730 ± 370	–0.294 ± 0.004
2HT125N	550–240	235–225	215	102.13	204.3	7890 ± 670	–0.280 ± 0.008

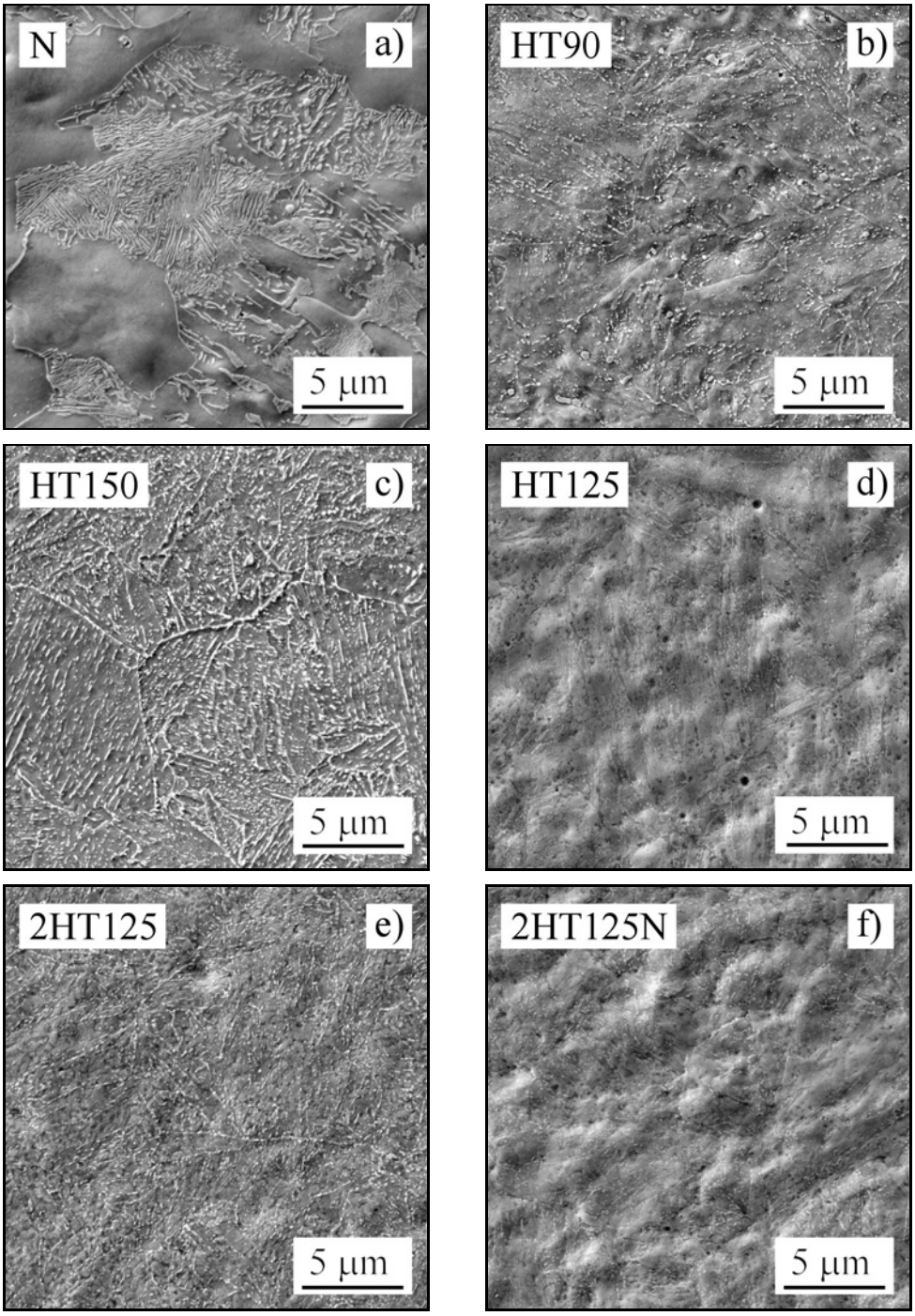

Fig. 3. Microstructure of material AISI 4130 for six different states of heat treatment: (a) N, (b) HT90, (c) HT150, (d) HT125, (e) 2HT125, and (f) 2HT125N (SEM, magnification 5000×).

dences in Fig. 2, i.e., oblique lines. The second interval is the transition region between the oblique and horizontal lines. The fatigue limit was set to 5–10 MPa below the second interval. The values of fatigue life parameters A and b in Eqs. (1) and (2) were determined by regression analysis, and their values and standard errors are listed in Table 1.

The fatigue properties were related to the evolution of microstructure reached by heat treatment (see SEM micrographs in Fig. 3). The observed microstructure is shown at a relatively high magnification. Fig. 3a shows a normalised state of AISI 4130 steel denominated as N exhibiting ferritic-pearlitic microstructure. Other heat treatments (HT90 and following) resulting in a hardened state exhibit the microstructure of tempered martensite. The pictures show a needle-like structure with martensitic plates arranged in packets formed based on the primary austenitic grains. A

Table 2. The phase composition, Prior Austenitic Grain Size (PAGS), and Maximum Feret Diameter (MFD) of martensitic laths for various heat treatment states evaluated based on EBSD analysis

Material state	Carbides (%)	Austenite (%)	Ferrite/Martensite	PAGS (μm)	MFD of martensite (μm)
N	2.10	0.03	Rest	–*	9.4 ± 8.2
HT90	1.14	0.27	Rest	20.5 ± 4.4	4.4 ± 3.6
HT125	1.61	0.61	Rest	22.0 ± 4.6	4.9 ± 3.5
HT150	0.77	0.08	Rest	24.5 ± 6.0	6.5 ± 3.3
2HT125	0.38	0.42	Rest	25.3 ± 5.9	6.8 ± 4.0
2HT125N	0.46	0.06	Rest	19.0 ± 3.8	4.8 ± 3.0

* was not evaluated

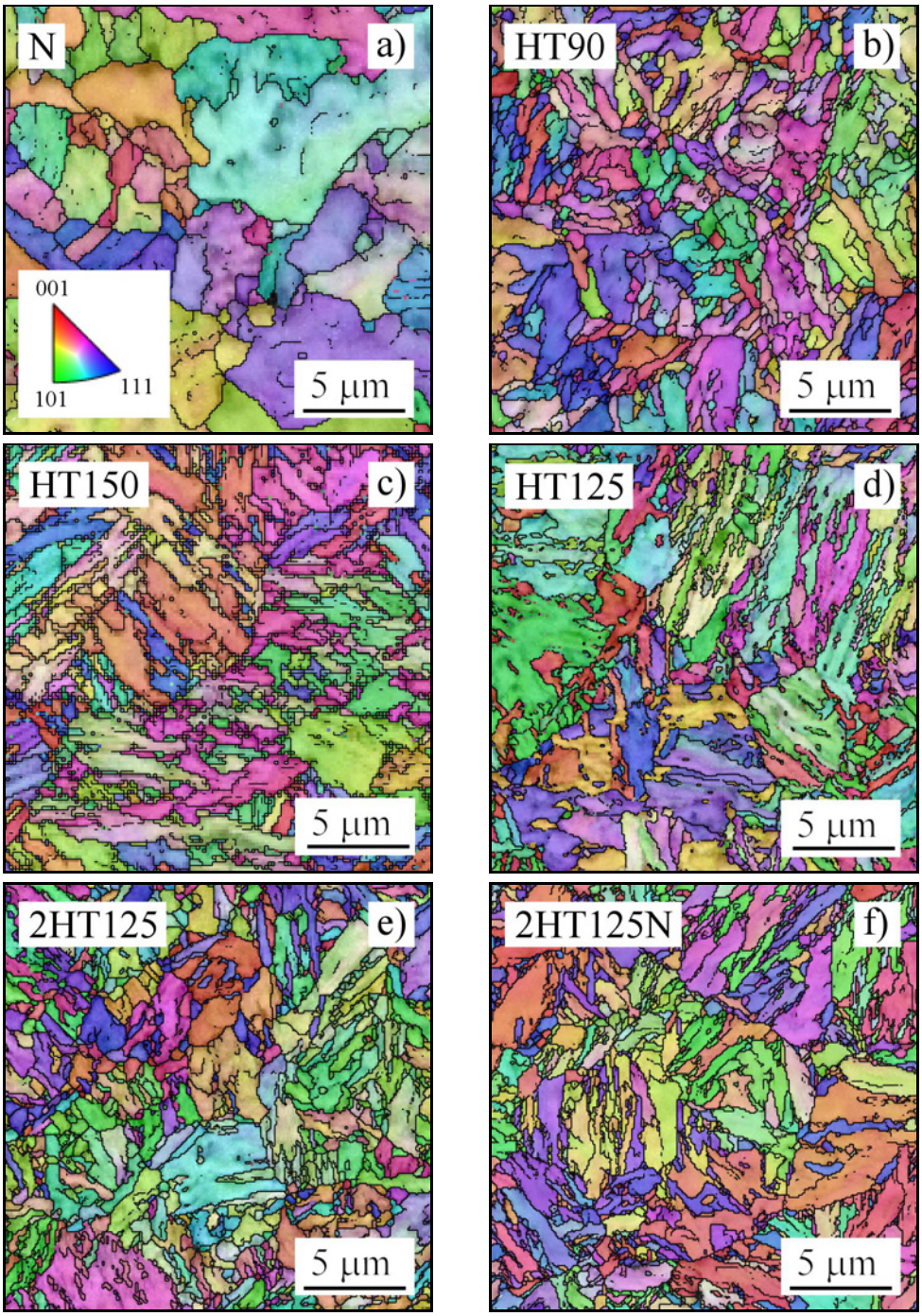

Fig. 4. EBSD maps in IPF colours in Z-axis orientation of material AISI 4130 for six different states of heat treatment: (a) N, (b) HT90, (c) HT150, (d) HT125, (e) 2HT125, and (f) 2HT125N.

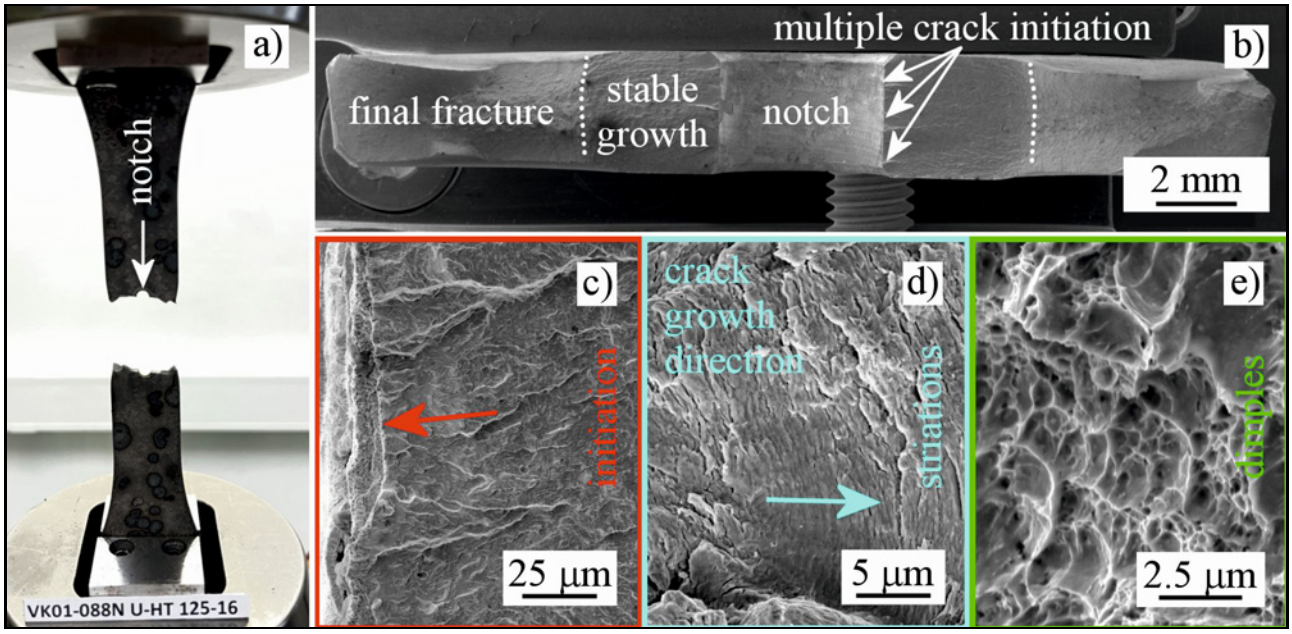

Fig. 5. Fractography of HT125 specimen 16 (N_f = 11.000, σ_a = 550 MPa): (a) specimen after test termination gripped in loading machine, (b) overview of the fracture surface, (c) detail of one initiation point, (d) detail of striations, arrow indicates crack growth direction, and (e) ductile dimple pattern from final fracture area.

small amount (from 0.5 up to 3 %) of fine carbides (white particles up to 500 nm in size) were found distributed relatively homogeneously in the microstructure both on the surface and inside the martensitic plates (see Figs. 3b–f).

The microstructural observation was also supplemented by electron backscattered diffraction (EBSD) analysis of all material states for determination of phases, i.e., the number of carbides and the possible presence of retained austenite in the microstructure after heat treatment (see Table 2). All material states perfectly fulfilled the user's requirement (Aircraft Industries) that after heat treatment, the amount of residual austenite was not greater than 10 %, whereas the highest value of 0.61 % was reached in the case of HT125 treatment. The highest amount of carbide phase present in the microstructure, reaching a value of 2.1 %, was observed in the normalised state with ferritic-pearlitic microstructure. In the hardened state, the highest value of 1.61 % was reached in the case of HT125 treatment.

In addition, EBSD maps using an inverse pole figure (IPF) colouring mixed with grain boundaries and band contrast were created (see Fig. 4) and used for microstructure assessment. The random orientation of individual grains in IPF maps confirms no texture in the material. The prior austenite grain size (PAGS) influences the martensitic transformation through the nuclei density provided by the grain boundary area and through strengthening the austenite phase as the transformation progress [8]. According to colour contrast and geometrical pattern from EBSD analysis, it was possible to estimate the PAGS. Results for all analysed specimens are listed in Table 2, where the value varied between 19 and 25 µm.

EBSD patterns reveal individual grains in microstructure more clearly than any ordinary SEM image in terms of grain boundary location, so it was possible to evaluate the size of martensitic laths. We used the recalculation of the grain area in terms of maximum Feret diameter (MFD). The evaluation was performed on at least 2000 grains for each material state. Based on the MFD parameter, it was possible to compare the martensitic substructure for individual heat treatments (see Table 2). The results show that the normalised state (N) exhibits a complete transformation of austenitic grains into ferritic-pearlitic grains with a size of approximately 9.4 µm. The assessment of martensitic microstructure for hardened states led to the following results. In the case of heat treatment HT90, HT125, and 2HT125N, a nearly similar size of martensite was observed, having an MFD between 4.4 and 4.9 µm. The remaining material states HT150 and 2HT125 exhibited coarsening of martensitic lats manifested in increased MFD to 6.5 and 6.8 µm, respectively. MFD values are defined as the distance between the two parallel planes restricting the object perpendicular to the selected direction.

Specimens were observed after test termination from a fractographical point of view to confirm the initiation of a fatigue crack from the central notch of the specimen. Figure 5a shows a fractured specimen in the fatigue machine where crack growth is perpendicular to the specimen, and the loading axis is visible. Figure

5b shows the fracture surface with simultaneous multiple initiations of fatigue cracks on both sides at the edge of the central notch. The growth of fatigue cracks was first stable (see flat part of fracture surface) followed by sudden final fracture exhibiting a small magnification roof-like pattern, typical for metal sheets. Figure 5c shows a picture of one initiation point in higher magnification. Figure 5d shows striations typical for stable fatigue crack growth [9]. The detail from the area of the final fracture (see Fig. 5e) shows ductile dimple morphology.

4. Conclusions

The results of the study of the fatigue life in a wide interval of the number of cycles to fracture of AISI 4130 steel on flat test specimens with a central notch prepared in six variants of heat treatment can be summarised as follows:

– The lifetime variance for all heat-treated states was relatively low, which enables a good description of the lifetime curve in the form of the dependence of the maximum stress in the cycle σ_{max} on the number of cycles to fracture N_f in a bi-logarithmic representation.

– The dependence of σ_{max} versus N_f in the bi-logarithmic representation can be characterised by two linear branches (oblique and horizontal) connected by a short transition area. The oblique branch corresponds to a power law dependence, while the horizontal branch characterises the conventional fatigue limit for the number of cycles 5×10^6.

– Fatigue life parameters A and b, describing oblique linear branches of the dependence σ_{max} vs. N_f, were evaluated using regression analysis for all material states. The conventional fatigue limits were also determined. The highest value of the maximum stress at a fatigue limit of 225 MPa for the number of cycles 5×10^6 exhibited material in the HT125 state.

– Heat treatment HT125 reaches the best fatigue limit, approximately 50 % higher than for the N state and 5–15 % better than for other hardened states.

– The best fatigue properties, i.e., the highest fatigue limit of the hardened state HT125, can be attributed to the most appropriate microstructure when fine needles of tempered martensite were created with a homogeneous distribution of fine carbide phase in the amount of approximately 1.6 % in the grain interior.

– Fractography observation revealed the symmetrical multiple initiations of fatigue cracks from the central notch, stable fatigue crack growth followed by a final fracture with the ductile pattern.

Acknowledgements

The financial support for conducting the research and/or preparing the article was provided by the TACR agency. Results of the research were presented at the XXI International Colloquium on Mechanical Fatigue of Metals (ICMFM 21) held on 22–24 May 2023 at the Institute of Physics of Materials, the Czech Academy of Sciences in Brno, Czech Republic. The presentation given by Jakub Poloprudský was awarded.

This project is financed from the state budget by the Technology Agency of the Czech Republic and the Ministry of Transport within the DOPRAVA 2020+ Programme under project no. CK02000025 Advanced welded structures for enhanced operational safety in aviation.

References

[1] H. J. Hucek, A. R. Elsea, A. M. Hall, Evolution of Ultrahigh-strength, Hardenable Steels for Solid-propellant Rocket-motor Cases, first ed., Defense Metals Information Center, Battelle Memorial Institute, 1961.

[2] H. Mollazadeh, R. Noruzi, M. Eskandarzade, A study of fatigue properties of steel AISI4130 (30KhMF) after upset welding, Metal Science and Heat Treatment 57 (2015) 52–56. https://doi.org/10.1007/s11041-015-9834-1

[3] The Metallic Materials Properties Development and Standardization (MMPDS) Handbook-16, Battelle Memorial Institute, 2021.

[4] ASTM E 466-96, Standard Practice for Conducting Force Controlled Constant Amplitude Axial Fatigue Tests of Metallic Materials, ASTM International, 1996.

[5] ASTM E 739-10, Standard Practice for Statistical Analysis of Linear or Linearized Stress-Life (S-N) and Strain-Life (ε-N) Fatigue Data, ASTM International, 2015.

[6] K. M. Rajan, P. U. Deshpande, K. Narasimhan, Effect of heat treatment of preform on the mechanical properties of flow formed AISI 4130 Steel Tubes – a theoretical and experimental assessment, Journal of Materials Processing Technology 125 (2002) 503–511. https://doi.org/10.1016/S0924-0136(02)00305-9

[7] A. Emamian, A. Emamian, A. H. Kowkabi, Effects of fillerwire composition along with different pre- and post-heat treatment on mechanical properties of AISI 4130 welded by the GTAW process, Materials Sciences and Applications 1 (2010) 135–140. https://doi.org/10.4236/msa.2010.13022

[8] C. Celada-Casero, J. Sietsma, M. J. Santofimia, The role of the austenite grain size in the martensitic transformation in low carbon steels, Materials & Design 167 (2019) 107625. https://doi.org/10.1016/j.matdes.2019.107625

[9] P. Maruschak, R. Vorobel, O. Student, I. Ivasenko, H. Krechkovska, O. Berehulyak, T. Mandziy, L. Svirska, O. Prentkovskis, Estimation of fatigue crack growth rate in heat-resistant steel by the processing of digital images of fracture surfaces, Metals 11 (2021) 1776. https://doi.org/10.3390/met11111776